

Modeling of mixed-phasing antenna-plasma interactions on JET A2 antennas

D. A. D'Ippolito and J. R. Myra

Lodestar Research Corporation, Boulder, Colorado, USA

P. M. Ryan

Oak Ridge National Laboratory, Oak Ridge, Tennessee, USA

**E. Righi,¹ J. Heikkinen,² P. U. Lamalle,³ J.-M. Noterdaeme,⁴ and
Contributors to the EFDA-JET Workprogramme**

EFDA-JET, Abingdon, Oxfordshire, United Kingdom

¹EFDA-CSU Garching, Germany; Present address: European Commission, Brussels, Belgium.

²Association Euratom-Tekes, VTT, Finland.

³EFDA-CSU Culham, UK & LPP-ERM/KMS, Brussels, Belgium.

⁴IPP, Euratom Association, Garching, Germany.

June 5, 2002; revised August 23, 2002

(submitted to Nuclear Fusion)

Modeling of mixed-phasing antenna-plasma interactions on JET A2 antennas

D. A. D'Ippolito and J. R. Myra
Lodestar Research Corporation, Boulder, Colorado, USA

P. M. Ryan
Oak Ridge National Laboratory, Oak Ridge, Tennessee, USA

E. Righi¹, J. Heikkinen², P. U. Lamalle³, J.-M. Noterdaeme⁴, and
Contributors to the EFDA-JET Workprogramme
EFDA-JET, Abingdon, Oxfordshire, United Kingdom

Abstract

The use of mixed (monopole-dipole) phasing of a set of ICRF antennas is potentially useful to optimize tokamak performance. However, recent mixed-phasing experiments on JET, described here, showed undesirable antenna-plasma interactions under certain circumstances. A possible physical mechanism to explain the experimental results is discussed, viz. rf-driven dc parallel currents flowing between adjacent antennas with different phasings can lead to arcing on the antenna with the largest sheath voltage. Means of controlling the interaction are discussed.

PACS Numbers: 52.40.Fd, 52.40.Kh, 52.50.Qt, 52.55.Fa

E-mail: dasd@lodestar.com

¹ EFDA-CSU Garching, Germany; Present address: European Commission, Brussels, Belgium.

² Association Euratom-Tekes, VTT, Finland.

³ EFDA-CSU Culham, UK & LPP-ERM/KMS, Brussels, Belgium.

⁴ IPP, Euratom Association, Garching, Germany.

1. Introduction

The use of mixed-phasings for a set of ion cyclotron range of frequency (ICRF) antennas is potentially useful to extend the control possibilities of the ICRF for optimizing tokamak performance. Dipole antennas are routinely employed to heat the core plasma without perturbing the edge, whereas monopole antennas can be used to modify edge and scrape-off-layer (SOL) properties by driving edge convection [1]. It has been suggested that the rf-driven convection can affect H-mode properties, such as the particle confinement time and the Edge Localized Mode (ELM) repetition rate, and reduce the divertor heat load by broadening the SOL [1, 2]. The convection may also be a useful tool in basic physics studies, e.g. by perturbing edge and SOL turbulence. To be successful, it must be possible to operate in mixed-phasings without deleterious interactions between adjacent antennas and without seriously degrading the plasma performance.

Mixed-phasing experiments have been carried out recently on JET for L-mode plasmas using the A2 antennas, and undesirable antenna-plasma interactions were observed under some conditions. In particular, phasing the four antennas alternately in monopole (0000) and dipole ($0\pi0\pi$) around the torus produced a heavy interaction with one monopole antenna; the strong interaction region was connected by magnetic field lines to an adjacent dipole antenna. A similar interaction was not observed using either pure monopole or pure dipole phasing in the L-mode shot, nor was it observed with mixed phasing in one H-mode shot. A sheath analysis described in this paper suggests that the observed interaction in L-mode is due to arcing [3, 4], induced by a large dc sheath potential difference and resulting current flow [5], between antennas with mixed phasings. If this is indeed the mechanism responsible for the observed interactions, our analysis suggests that future mixed-phasing experiments may be successful in H-mode plasmas, which have lower density near the antenna.

A number of previous papers have considered radiofrequency (rf) sheath effects on ASDEX[6], JET [1,7-9], TFTR [10,11], and Tore Supra [12,13] including sputtering of impurities by ions accelerated in rf sheaths [6-10], sheath-induced perpendicular convection [1,10,13], sheath power dissipation [9] and hot spots [11,12]. These effects are determined mainly by the local rf sheath potential at a given antenna and are relatively insensitive to the boundary condition at the opposite end of the field line. The TEXTOR [5,14] and ASDEX [15-17] groups have also pointed out the importance of non-local sheath effects, such as the

generation of dc parallel currents [5,14], which depend on the relative sheath potentials and flux tube surface areas at both ends of the field line. In the present paper, we extend our previous work to include the generation of parallel currents by asymmetric sheaths, and we will show that non-local sheath effects are necessary to understand the recent JET mixed-phasing results.

The plan of this paper is as follows. The experimental results are summarized in Sec. 2, and the theoretical model is described in Sec. 3. The model describes the formation of asymmetric rf sheaths at adjacent antennas, the resulting parallel and perpendicular current flow, and the arcing threshold. A summary and discussion is given in Sec. 4.

2. Experimental results

An experiment to study the effect of antenna phasing on the ICRF heating efficiency of plasmas and the effect of rf sheath potentials on SOL properties was carried out during the 2000 EFDA-JET Workprogram (C3 Campaign, November 2000). The four 4-strap A2 ICRF antennas [18] (called Modules A, B, C, D) were used to heat H minority ions in a D plasma with various combinations of monopole (0000) and dipole ($0\pi0\pi$) phasings at $\omega = \omega_{cH} = 42$ MHz. Here, the notation (0000) implies that the phase difference between the currents in adjacent straps is 0 for all four straps, whereas ($0\pi0\pi$) implies a phase difference of π . The target was a standard flux expansion plasma with $I_p = 2.6$ MA, $B_T = 2.8$ T, $n_e = 2 \times 10^{19} \text{ m}^{-3}$ (before application of ICRF). The plasma-antenna distance was kept constant at 4 cm. This experiment yielded interesting data on antenna-plasma interactions in mixed-phasing operation.

In shot #52673 the phasing was chosen to have toroidally alternating monopole and dipole antennas with Mod. C (0000) viewed by the CCD camera to monitor possibly damaging interactions with the first wall structures (poloidal limiters, antenna septum, railings and Faraday screen). The time sequence of the rf power and relevant core and edge diagnostics is shown in Figs. 1 and 2. The rf power was ramped up to 2 MW in 2 s on all four antennas (8 MW total) at the same time, followed by 2 s periods of alternated 0000 (Mod. A and C) and $0\pi0\pi$ (Mod. B and D) with 2 MW per antenna; all modules (8 MW) were on again for 2 s and then ramped down to zero power. The plasma remained in L-mode for the duration of this shot.

Strong interactions with the antenna structure of Mod. C (0000), with release and acceleration of particulate matter into the plasma, were visually observed from the torus CCD camera at several times in the discharge when mixed phasings were present. Figure 2 shows the corresponding data from edge plasma diagnostics. When the first interaction started (at 17.8 – 18.04 s), sudden increases of edge density (measured at $R = 3.75$ m with the high temporal resolution FIR interferometer) and D_α line intensity were observed, and these coincided with a very localized (spatially and temporally) increase in edge T_e (as seen by the heterodyne radiometer). The increase in edge T_e rapidly decreased with decreasing R and was not present for $R < 3.80$ m. (The separatrix position, from the T_e profile, is $R_{\text{sep}} \cong 3.83$ m.) Following the n_e , T_e spikes there was a release of oxygen, carbon and (to a lesser degree) nickel in the plasma. The analysis of this data suggests that intense localized heating released first wall material, giving rise to a local increase of density and high Z impurities, during the high-power ramp-up with mixed-phasings. The central line-averaged density also increased during the antenna interaction, as shown in Fig. 1.

No interactions were observed during the periods of exclusively monopole or dipole phasing. In the second period with mixed-phasings, another interaction was visually observed, but no spikes in either n_e , T_e or high Z material line intensities were present, with the possible exception of a small increase in the CIV line. The reduced severity of the second interaction was probably due to the unsteady power delivered by Mod. D during this time segment.

The camera showed the interaction area on Mod. C to be roughly $\frac{1}{2}$ of the antenna, and this region is connected to Mod. D by the field line mapping. The reciprocating probe data indicated the presence of strong sheath rectification. At the time when the first interaction on Mod. C occurred, the rf power showed evidence of generator tripping [see Fig. 1] and the traces of C, O, and Ni impurities [see Fig. 2] and line-averaged Z_{eff} [not shown] showed sudden peaks, all of which are consistent with the presence of arcing.

There is some preliminary evidence (from a single shot) that the observed antenna interaction does not occur in H-mode plasmas. In shot #52678, 6 MW of ICRF power in dipole phasing and 2 MW of NBI power were injected into the same target plasma (as in the earlier shot) to obtain an ELMy H-mode. Subsequently 1.5 MW of ICRF heating was applied using the Mod. C antenna in monopole phasing. During the use of mixed phasings in this H-mode shot, no interaction with the Mod. C was observed with the CCD camera, although the intensity of the CIII and CIV lines did increase in coincidence with it. If this result is

confirmed in future experiments, it suggests that the lower edge density of H-mode plasmas may turn off the interaction mechanism. We will show that this hypothesis is consistent with the theoretical model.

More experiments will be needed to confirm whether the antenna-plasma interactions are reduced in H-mode, and whether a useful “window” exists in which the monopole rf power is small enough to avoid these interactions but large enough to affect the H-mode.

3. Theoretical model

A brief summary of our model is as follows. In mixed-phasing ICRF antenna operation, the magnitude of the rf sheath potential is much larger at the antenna with monopole (0000) phasing than at the one with dipole ($0\pi0\pi$) phasing. This asymmetry can drive significant currents on field lines which connect the antennas, with the monopole antenna serving as the cathode on which the arc forms. The simplest picture is to regard the two antennas as probes or capacitor plates biased to different rf voltages and directly connected by magnetic field lines. The actual picture is more complicated, because the antennas are separated by poloidal limiters and the current must flow radially around the limiters. The radial part of the current path is supplied by rf-driven convection (which explains why the effect requires that both antennas be powered). If the parallel current to the monopole antenna exceeds a threshold condition, an arc can be triggered, causing damage to the antenna surface. In the following sub-sections, we give a brief overview of rf sheath physics and then describe the elements of the model in more detail.

3.1 RF sheath physics

As background for the following analysis, we begin this section with a brief overview of rf sheath physics. The formation of rf sheaths is induced by the action of an rf field with a substantial component E_{\parallel} parallel to \mathbf{B} . In the vicinity of a material boundary, electrons are accelerated out of the plasma by E_{\parallel} faster than the heavier ions, and a confining dc (“rectified”) sheath potential Φ develops to confine electrons and restore equilibrium quasineutrality [6,14,19,20], leaving narrow sheaths of positive space charge and intense electric fields near the contact points. Outside the sheaths, the potential Φ is nearly constant along the equilibrium magnetic field but varies rapidly across it, because the field line contact points with material surfaces change rapidly with perpendicular coordinates x and y . The spatial variation of $\Phi(x,y)$ in the plane perpendicular to \mathbf{B} drives rapid $\mathbf{E}\times\mathbf{B}$ convection

[1,10,13] which increases the flux of plasma density and current to the antenna and thereby enhances the strength of the antenna-plasma interactions. During high power operation the induced sheath potential is large ($e\Phi \gg 3T_e$) and the energy $Ze\Phi$ of ions accelerated in the rf sheaths can be in the range 0.5 - 2 keV where the sputtering yield of metal impurities peaks, leading to greatly enhanced impurity influxes from the antennas, limiters or other nearby surfaces [6-10]. The energetic ion flux out of the plasma also produces a parasitic power loss (“sheath power dissipation”) [25], which under extreme conditions can significantly reduce the heating efficiency [9] and cause overheating of the antenna structure [11,12]. These effects are determined mainly by the *local* rf sheath potential at a given antenna and are relatively insensitive to the boundary condition at the opposite end of the field line. Another sheath effect which plays an important role in the present analysis is the generation of dc parallel currents, as first observed on TEXTOR [5,14]. The sheath-generated currents are a *non-local* effect because they depend on the relative sheath potentials and flux tube surface areas at both ends of the field line.

For fast wave antennas, the E_{\parallel} field component arises because of a mismatch between the orientations of the equilibrium magnetic field and the antenna structure [7,11,19] and because of feeder effects [11]. In carrying out a sheath analysis, it is useful to introduce the sheath driving voltage $V = \int ds E_{\parallel}$, where the integral is taken along the field line between contact points with material surfaces. By Faraday’s Law, the sheath voltage on a given field line segment intersecting the antenna can also be regarded as proportional to the rf magnetic flux linked by the circuit consisting of the field line and the antenna [7]. Thus, in a multiple current strap antenna V is sensitive to the cancellation of the E_{\parallel} fields (or equivalently the rf magnetic flux) produced by toroidally adjacent current straps, and hence to the phase difference between straps; the voltage V is largest for a phase difference of 0 (“monopole” phasing, no cancellation) and smallest for a phase difference of π (“dipole” phasing, maximum cancellation). It is also useful to define the rectified potential Φ_0 obtained from 1D sheath theory (i.e. ignoring perpendicular motion) by $\Phi_0 = C_r V$. If V is defined to be the 0-to-peak value and we assume high density (full space charge) and high voltage ($eV/T_e \gg 1$), computer simulations [20] yield a value $C_r = 0.6$ for the rectification coefficient in a 1D model with fluid ions and Maxwell-Boltzmann electrons. The 2D rectified potential Φ will differ from Φ_0 due to effects of perpendicular currents, but in practice $\Phi \approx \Phi_0(x,y)$ is usually a good order-of-magnitude estimate.

The computation of V and Φ as a function of phasing for the JET A2 antennas is discussed in Sec. 3.2. An analytic model to estimate the resulting sheath-driven parallel current is given in Sec. 3.3, and the rf convection of this current around the antenna limiters is described in Sec. 3.4. Finally, Sec. 3.5 discusses the effect of the sheath-driven current on stimulating arcing at the monopole antenna to complete the present model of the JET mixed-phasing experiments.

3.2 Rf sheath asymmetry

The first step in the model is to use the results of a numerical sheath analysis to show that there is a large asymmetry in the rf sheath voltages between the monopole and dipole phased JET A2 antennas.

In previous work, the rf sheath distribution was analyzed for the flatbed mockup [21] of a single 4-strap JET A2 antenna using the combined ARGUS [22] and ANSAT [23] codes. The unpublished results of this study include the rf sheath distribution on the antenna for both phasings of interest here operating at a frequency of 44 MHz. The ANSAT code calculates the rf sheath driving voltage $V = \int ds E_{\parallel}$ defined in the previous section. In one series of calculations we compared monopole (0000) and dipole ($0\pi 0\pi$) phasings assuming that the side slots in the frame of the original flatbed mockup were covered by “flux excluders.” This is the version that most closely resembles the present JET A2 antenna (taking into account the modifications made in 1996). A magnetic field angle of 15 degrees with respect to the toroidal direction was assumed for the calculations reported here. One aspect of the mockup antenna that differs from the actual A2 antennas is that the Faraday screen (FS) bars in the mockup are horizontal, whereas the FS bars in the A2 antennas are more closely aligned with the magnetic field. Thus, the contributions of the gap and front face sheath voltages were overestimated in the numerical simulation (by about a factor of 2) but the antenna-limiter sheaths (which are independent of FS angle and have the largest voltages) were calculated correctly. The degree of asymmetry between the monopole and dipole sheaths, which is the main point of interest here, is also relatively insensitive to the screen angle.

The sheath voltage was calculated for field lines at various radial (x) and poloidal (y) positions near the antenna. In this discussion, and in Fig. 3, all sheath voltages will be given in arbitrary code units (a.u.). The conversion to physical units is discussed subsequently. As a diagnostic, we computed the poloidal distribution of the rf sheath voltage $V(y)$ on field lines

just in front of the FS tangency surface (see Fig. 3). Taking the maximum value of $V(y)$ as a rough measure of the strength of the sheaths, we find that $V_{\max} \approx 6.5$ a.u. in monopole phasing and $V_{\max} \approx 2.2$ a.u. in dipole phasing. By this measure, the ratio of the sheath voltages at the monopole and dipole antennas is roughly a factor of 2-3. (This is a rough estimate, because ratio of the sheath voltages at the two contact points for a particular field line depends sensitively on its poloidal position.) We conclude from this modeling that for typical field lines there is a large asymmetry between the monopole and dipole sheath voltages.

In order to convert the code units to physical voltages, we note that the voltage drop from top to bottom of the current strap, $V_a = \int dy E_y$, is 14.0 in code units. Here, E_y is the electric field component along the axis of the current strap and the integral is taken in the vacuum region just in front of the current strap. Thus, the maximum ratio of $C_v \equiv V/V_a$ is $6.5/14 \approx 0.46$ in monopole phasing and $2.2/14 = 0.16$ in dipole phasing. For the experiments of interest here with resonant ($1/4$ wavelength) straps, the “0 to peak” antenna voltage V_a (kV) is related to the rf power P_{rf} (MW) by

$$V_a \text{ (kV)} = Z_0(\Omega) \sqrt{\frac{2P_{\text{rf}} \text{ (MW)}}{N R_c(\Omega)}}, \quad (1)$$

where $Z_0(\Omega)$ is the characteristic impedance of the feed line, $R_c(\Omega)$ is the antenna coupling resistance per strap, and N is the number of straps. Finally, the rectified sheath potential Φ is defined in terms of the 0-peak antenna voltage by $\Phi \equiv 0.6 V = 0.6 C_v V_a$. Here, the factor 0.6 is the sheath rectification factor from the time-averaged quasineutrality condition [20] and C_v is a factor describing the amount of magnetic flux cancellation among the current straps in a given antenna module. Using the parameters $N = 4$, $Z_0 = 30\Omega$, the resistance values [24] $R_c = 2\Omega$ (dipole) or 5Ω (monopole) and $P_{\text{rf}} = 2$ MW, we obtain the typical sheath voltages in kV shown in Table 1. As noted above, these voltages are a worst case estimate, because the mockup antenna does not have FS bars aligned with the local magnetic field. Even if we reduce the computed voltages by a factor of 2 to take into account this effect heuristically, we see that both monopole and dipole sheath voltages exceed 1 kV. This fact will be important in computing the radial current flow in Sec. 3.4.

Table 1 Summary of rf sheath rectified voltages for two phasings
(at a nominal power level of 2 MW per module)

phasing	$R_c(\Omega)$	$V_a(\text{kV}, 0\text{-peak})$	$\Phi(\text{kV})$
0000	5	13	3.7
0 π 0 π	2	21	2.0

3.3 Parallel current flow

The second part of the model is to show that a sheath voltage asymmetry can produce a parallel current flowing between the antennas. We also need to know its direction and to estimate its magnitude.

Sheath-driven currents flowing between powered ICRF antennas and the belt limiter have been observed on TEXTOR [5,14]. If the electron mean free path is sufficiently long compared to the parallel separation of the two antennas ($L_{\parallel} < \lambda_e$), we can apply traditional sheath theory to calculate the current. The simplest model is to represent the two antennas as two capacitor plates with rf bias voltages $V_{\text{rf}j}$ ($j = 1, 2$) connected by field lines immersed in a plasma. For simplicity, the plates are assumed to have equal areas ($= A$) projected normal to the field lines, and the ground potential is taken to be the time-averaged potential of the plates. (In general, A represents the antenna area projected normal to the field lines.) A symmetric version of this model with $V_{\text{rf}1} = V_{\text{rf}}$ and $V_{\text{rf}2} = -V_{\text{rf}}$ is described in the Appendix of Ref. [25]. The key simplification in the model that allows an analytic solution for the plasma potential and current is that only dc and $\cos\omega t$ variations of the plasma quantities are retained. The small higher harmonic contributions are neglected. In this paper, we generalize the model to include the case where the rf driving voltages on the two plates are unequal and a time-averaged current flows between the plates.

The calculation is briefly summarized as follows. In this model the instantaneous plasma potentials V_{pj} relative to the two plates ($j = 1, 2$) and the plasma potential V_0 (relative to ground) are related to the driving voltages by

$$V_{\text{pj}} = V_0 - V_{\text{rf}j} \cos \omega_j t, \quad (2)$$

where ω_j is the rf frequency at the j th plate. (It is not necessary to assume that the two plates are in phase or oscillating at the same frequency because in this model the dc current will depend only on time-averaged quantities local to each sheath.) Suppressing the subscript j , the plasma potential V_0 can be expanded as $V_0 = V_{00} + V_{02} \cos 2\omega t + \dots$. Note that there is no $\cos \omega t$ contribution to the plasma potential because of the plasma rectification effect [19, 20, 26]. Here, we neglect the small V_{02} and higher harmonic terms and let $V_0 = V_{00}$ represent the time-averaged plasma potential.

We write expressions for the ion, electron, and total current flowing to each plate, adopting the sign convention that ion current flowing into plate 2 is positive. The requirement that the time-averaged net current lost from the system must vanish (by quasineutrality) determines the dc plasma potential V_0 . Defining $x_0 = eV_0/T_e$ and $\xi_j = eV_{rfj}/T_e$ and using a Bessel's function identity to express the exponential dependence of the electron current on the potentials, we can write the quasineutrality condition in the form

$$x_0 = x_B + \ln \left(\frac{I_0(\xi_1) + I_0(\xi_2)}{2} \right), \quad (3)$$

where x_0 is a measure of the dc plasma potential relative to ground and x_B is the usual Bohm sheath potential, $x_B = \ln(v_e/(2\pi)^{1/2}c_s)$. Eq. (3) recovers the results of Ref. [25] when $|\xi_1| = |\xi_2|$. Another check of Eq. (3) for the case $\xi_1 = -\xi_2 \equiv \xi$ is obtained by taking the large voltage (asymptotic) limit $\xi \rightarrow \infty$ of the Bessel's functions in Eq. (3). This yields the approximate relation $x_0 \approx \xi$, which can be rewritten as $V_0 = V_{rf} = 0.5 (V_{rf1} - V_{rf2}) \equiv 0.5 V$ for this case, where V is the total sheath driving voltage as defined in the previous sections. The sheath rectification coefficient 0.5 in the analytic model is close to the coefficient 0.6 obtained by computer simulations of the 1D sheath problem [20].

One can also determine the net throughput current, i.e. the current flowing around the circuit, from this model. We find that the time-averaged throughput current (which is probably the relevant quantity for arcing) is given by

$$\langle I_{\text{thro}} \rangle = I_s \frac{I_0(\xi_1) - I_0(\xi_2)}{I_0(\xi_1) + I_0(\xi_2)}, \quad (4)$$

where $I_s = Aen_e c_s$ is the ion saturation current.

Whereas x_0 , and hence the potential V_0 , in the quasineutrality relation (3) is relatively insensitive to the asymmetry between ξ_1 and ξ_2 , the net current $\langle I_{\text{thro}} \rangle$ in Eq. (4) vanishes when $|\xi_1| = |\xi_2|$. *In our theory, this is the fundamental reason why the mixed-phasing case differs from the case where all antennas have the same phasing.*

We can use Eq. (4) to estimate the requirements for significant current. Taking the extreme asymmetric limit, $\xi_1 = \xi$, $\xi_2 = 0$ gives

$$I_t \equiv \frac{\langle I_{\text{thro}} \rangle}{I_s} = \frac{I_0(\xi) - 1}{I_0(\xi) + 1} \sim 1 \quad (5)$$

where the last form is the asymptotic large- ξ limit. Evaluating $I_t(\xi)$, we find that the asymptotic limit is attained for modest values of the rf driving voltage ($\xi > 5$, which for typical parameters corresponds to a voltage greater than about 100 volts). Returning to the general case, it is also possible to plot the current vs. the degree of asymmetry. Taking $\xi_1 = (1-g)\xi$, $\xi_2 = -g\xi$, we show in Fig. 4 the normalized current I_t vs. g . It is seen that only a small amount of asymmetry is required in the high voltage limit ($\xi \gg 1$) for the current to saturate ($I_t = 1$).

To summarize, this model shows that an asymmetrically driven pair of rf sheaths draws a time-averaged current. The current flows to the side with the lowest instantaneous plasma potential V_{pj} ; this occurs at the plate with the largest rf driving voltage (V_{rfj}) at the point in the rf cycle when the rf driving voltage tends to cancel with the time-averaged potential. Thus, excess electrons flow to the high rf-voltage plate. The maximum magnitude of this current is the ion saturation current, and this value is achieved for modest rf voltages, $V_{\text{rf}} > 5T_e/e$. In this high voltage limit, only a small amount of asymmetry in the driving voltages is required to achieve significant currents. For typical temperatures ($T_e = 50$ eV) this requires $V_{\text{rf}} > 250$ V, a value much smaller than typical sheath driving voltages on the A2 antennas (see Table 1).

3.4 Radial current flow

The next step in developing the theory is to address the difficulty that the JET antennas are separated by poloidal limiters that extend radially a distance $\Delta x_L = 1.1$ cm in front of the FS tangency surfaces. This means that the simple picture of field lines directly connecting the two antennas (as in the capacitor plate model) is not applicable. However, the same physics of sheath-driven currents can be recovered if some means is found to provide a radial current

path around the limiters, restoring the complete circuit between the antennas. In fact, radial currents can be provided by rf-sheath-driven convective cells [1]. For high-power antennas with large (kV) sheath potentials, it was shown in Ref. [1] that the convective cells could extend over a significant fraction of SOL width and could carry radial currents.

The physics of rf convection is generic to ICRF antennas. Due to the complicated structure of the antenna and the Faraday Screen, the rf sheath driving voltage varies from one field line to another. The dc sheath potential $\Phi(x,y)$ resulting from the sheath rectification process tends to oscillate poloidally with the periodicity of the FS structure and to decay radially away from the antenna. The corresponding dc electric field pattern drives $\mathbf{E} \times \mathbf{B}$ convective cells which transport particles and current across the field lines. The convective cell equation is derived [1] from the field line average of the current equation, $\langle \nabla \cdot \mathbf{J} \rangle = 0$, where $\langle Q \rangle = \int ds Q/L_{\parallel}$ and the integral is taken along the field line between two axial boundaries in the SOL. This yields the vorticity equation

$$\frac{c^2}{B^2} n m_i \frac{d}{dt} \nabla_{\perp}^2 \Phi = \frac{J_{\parallel} \Big|_{-L_{\parallel}/2}^{+L_{\parallel}/2}}{L_{\parallel}} \equiv \frac{J(\Phi - \Phi_0)}{L_{\parallel}}. \quad (6)$$

Here, $d/dt = \partial/\partial t + \mathbf{v} \cdot \nabla$ with $\mathbf{v} = (c/B) \mathbf{b} \times \nabla_{\perp} \Phi$, Φ is the field-line averaged dc potential and we have dropped the brackets (e.g. $\langle \Phi \rangle \rightarrow \Phi$) for simplicity of notation, L_{\parallel} is the distance between the contact points, and $J(\Phi - \Phi_0)$ is the sheath current-voltage relation specifying the net current flowing out of the system as a function of the potential. For $\Phi = \Phi_0 \equiv V_0$ the net current vanishes, corresponding to the limit where one-dimensional sheath theory applies. For $\Phi - \Phi_0 \gg T_e/e$ the net current equals the ion saturation current, $J(\Phi - \Phi_0) \rightarrow n_i e c_s$, and the sheath problem is fully two-dimensional.

The radial current transport can be understood as follows. In the convective cell, the divergence of the parallel current is balanced by the contribution to $\nabla \cdot \mathbf{J}_{\perp}$ from the ion polarization drift, i.e. the terms on the lhs of Eq. (6). (The $\mathbf{E} \times \mathbf{B}$ drift, which dominates the particle convection, produces no charge separation and therefore does not contribute to the radial current.) Thus, the radial current is related to the change in the vorticity, $\omega = \nabla_{\perp}^2 \Phi$. The role of the time-derivative term in driving radial currents has been discussed in the context of Langmuir probe theory [27, 28] and would be important also for antennas in the high-Reynold's number turbulent regime. Here, we focus on the role of the convective term,

$\mathbf{v} \cdot \nabla \omega$, which plays a role in two-dimensional antenna sheath theory even in the laminar regime.

Note that $\nabla \cdot \mathbf{J} = 0$ implies that $J_x/L_x \sim J_{\parallel}/L_{\parallel}$, which can be rewritten as $J_x/J_{\parallel} \sim L_x/L_{\parallel} \ll 1$. This result implies that the radial current flux is comparable to the parallel current flux over the distance L_x , which is the radial scale length of Φ . Thus, even a small amount of radial current is sufficient to maintain the current path between antennas if the radial penetration of the convection is comparable to the radial protrusion Δx_L of the limiter, i.e.

$$L_x \approx \Delta x_L . \quad (7)$$

The nonlinear dependence of L_x on the rf sheath voltage can be estimated from Eq. (6). In making this estimate, we are interested in the two-dimensional case where $\nabla \cdot \mathbf{J}_{\perp} \neq 0$, implying that Φ deviates significantly from Φ_0 and $\mathbf{J} \approx n_i e c_s$. In contrast to the discussion in Ref. [1], we focus here on the role of the larger convective cells with poloidal extent L_y comparable to that of the antenna, so that $L_x \ll L_y$. With these approximations, Eq. (6) yields the following scaling for the penetration length of the radial current

$$\frac{L_x}{\rho_s} = \left(\frac{L_{\parallel}}{L_y} \right)^{1/3} \left(\frac{e\Phi}{T_e} \right)^{2/3} , \quad (8)$$

where $\rho_s = c_s/\Omega_i$ and $c_s = (T_e/m_i)^{1/2}$.

One must check whether Eq. (7) is satisfied for both monopole and dipole antennas. In estimating L_x , we use parameters typical of the dipole antenna, which has the weakest sheath voltage. Using $L_y = 20$ cm (from Fig. 3), $L_{\parallel} = 300$ cm, $T_e = 50$ eV, $e\Phi = 2000$ eV, and $B = 3$ T, Eq. (8) yields the estimate $L_x \approx 1.0$ cm, which is compared with $\Delta x_L = 1.1$ cm. We conclude that Eq. (7) is satisfied, implying that an order unity fraction of the radial current can extend beyond the limiter tangency surface. In this limit, the convection provides an effective radial current path around the limiters and restores the connection between adjacent antennas.

It should be emphasized that the convection must operate at both the monopole and dipole antennas in order for the circuit to be complete. *This may explain why the damage to the monopole antenna is only observed during the time that the dipole antenna is powered (even though significant asymmetry persists when the dipole antenna is unpowered).* For an unpowered antenna, the magnitude of the Bohm sheath potential ($e\Phi \approx 3T_e$) is too small and

its poloidal variation is too weak (L_y too large) to drive significant convection, with the result that the current path between the adjacent antennas is broken by the poloidal limiters.

3.5 Arcing threshold

The final element of the model is to understand how the arcing process [3, 4] depends on the dc parallel current flow and thus on the antenna phasing. First, it is useful to briefly summarize the essential results of the parallel current calculation given in Sec. 3.3, which shows that an asymmetry between the sheaths at the two ends of a field line can drive a parallel current, emphasizing here the dc behavior of the model. Thus, we consider a dc sheath model, where for simplicity two plates of equal area A are assumed to have a relative voltage V between them with the anode potential taken as ground. Here, the relative voltage is driven by the sheath rectification effects [19, 20, 26] discussed in Sec. 3.3 with $V_{rf1} = 0$ and $V = C_r V_{rf2}$, where $C_r \approx 0.6$ is the sheath rectification coefficient [20] defined in Sec. 3.1. The plasma potential profile $\Phi(x)$ between the plates is sketched in Fig. 5 for two cases. For $V = 0$, the plasma potential is positive with respect to the plates and the potential difference Φ between the plasma and the cathode is equal to the Bohm potential, $e\Phi \approx 3T_e$. In this situation, the electron and ion currents to each plate are equal to the ion saturation current, $I_s = nec_s A$, and there is no net parallel current flow. For $eV \gg 3T_e$, the cathode (ion collecting plate) is biased negatively with respect to the anode, so that essentially all of the electrons are reflected by the cathode sheath. In the large- V case, the ion current I_i to each plate is still equal to I_s , but the electron current is asymmetric: $I_e = 0$ to the cathode and $I_e = 2I_s$ to the anode. Thus, this picture has several elements which are important for understanding arcing: (1) an applied voltage difference between the plates is required to give a net parallel current; (2) for large voltages ($eV \gg 3T_e$) the magnitude of this current is equal to the ion saturation current and it flows to the cathode, and (3) the largest voltage difference between plasma and metal surface occurs at the cathode (here, the monopole antenna). The condition $eV \gg 3T_e$ is typically satisfied for powered ICRF antennas.

To increase the current beyond I_s requires that the electric field at the cathode surface becomes so strong locally that it can pull electrons off the surface and into the plasma, thereby initiating an arc. The characteristic electric field for ionization is so large that it far exceeds the average sheath electric field, but it can be attained locally at rough spots or protrusions that amplify the sheath electric field. At such a protrusion the emitting tip is subsequently

heated by Joule heating and the electron emission is increased by thermal field emission [4]. Also, electrons are emitted at much lower electric fields from contaminated surfaces than from clean ones [4]. Thus, the arc initiation process is somewhat random in space and depends sensitively on the surface conditioning. During the burning of the arc, the voltage required to sustain the arc (15 - 25 V) is much lower than that required to initiate it. Another requirement to sustain the arc is that the rate of local Ohmic heating by electron currents passing through the metal lattice exceed the rate at which the thermal conductivity of the material carries heat away. This condition is also dependent on the surface material and surface contamination, but for typical materials it leads to a minimum current of $I_{\min} = 1 - 10$ A to sustain an arc [3].

Combining the sheath and arcing physics, we obtain the following quantitative criterion for the possibility of rf-sheath-induced arcing:

$$I_s \equiv n e c_s f A_{\perp} > I_{\min} . \quad (9)$$

where I_{\min} is the minimum current to sustain an arc (discussed above), $A_{\perp} = A \sin \alpha$ is the projection of the sheath interaction area A normal to \mathbf{B} , and α is roughly the indentation angle of the V-shaped FS. Here, f is the fraction of the parallel current which flows between adjacent antennas due to the rf convection, completing the current path necessary for the arc to occur. Thus, $f = 0$ when one of the two antennas is unpowered ($J_{\perp} \rightarrow 0$) and the current there is blocked by the radial limiter. The opposite limit, $f \rightarrow 1$, is obtained when both antennas are powered and the rf sheath potential is strong enough that $L_x/\Delta x_L > 1$ at each antenna [see Eq. (8)]. One can also regard $f A_{\perp}$ as the area of the cathode antenna “wetted” by the rf convection and receiving the full saturation current. Taking $f = 1$, $n_e = 10^{11} \text{ cm}^{-3}$, $T_e = 50 \text{ eV}$, and $A_{\perp} \approx (100 \text{ cm})^2 \sin 3^\circ \approx 500 \text{ cm}^2$, we obtain the estimate $I_s \approx 40 \text{ A}$, which is the right order of magnitude to sustain an arc.

4. Summary and discussion

We conclude that the model described in this paper is a good candidate to explain the observed antenna interactions with mixed-phasings during the recent JET experiments. The key elements of the model are: (i) the rf sheath potential is much larger on the monopole antenna than on the dipole antenna; (ii) this asymmetry drives a parallel current of order the

ion saturation current; (iii) the complete current path requires a radial current to flow around the poloidal limiters, and this radial current is provided by the ion polarization current associated with rf convective cells; (iv) the arcing conditions are met most easily at the monopole antenna, viz. a large (negative) voltage difference between the material surface and the plasma, and a net parallel current which is large enough to sustain the arc.

There are several qualitative points of agreement between the model and the recent JET experiments:

1. the antenna interaction requires an asymmetry in the sheath potentials (and hence in the antenna phasings);
2. the interaction is observed on the antenna with the largest sheath potential (the monopole antenna);
3. there is a minimum rf power requirement on both antennas to trigger the effect (given by the requirement that the radial convection current be sufficiently large to complete the current path).
4. there is a lag time between the turn on of rf power and the observed interaction (the arc trigger involves heating the metal surface, which takes a finite time);
5. the model is consistent with generator tripping and release of high-Z material (due to arc currents).

Note that points 1 and 3 imply that no interaction is expected if either the monopole or dipole antennas are turned off or if all antennas have the same phasing, which is supported by the recent experimental observations. Finally, although sheath-driven SOL currents were not directly observed in these experiments, their existence has been measured on TEXTOR due to asymmetric field line connections between the rf antennas and the toroidal liner [5,14].

We mention in passing that the present model may also be consistent with older experiments carried out with the JET 2-strap A1 antennas. In those reversed-toroidal field experiments, rf-sheath-induced arcing was directly observed with a CCD camera when the A1 antennas were in monopole phasing [9]. By increasing the B field-FS mismatch angle and by using monopole phasing, these experiments created very large sheath voltages (of order 2 - 3 kV). Arcs were observed parallel to the reversed B field lines, accompanied by a sudden release of beryllium [9]. In these experiments, the field lines involved in the arcing probably connected an A1 antenna to a nearby limiter, again giving rise to an asymmetric situation with rf-driven currents.

Looking towards future experiments, it is useful to consider several questions in light of this model: Is there anything that can be done to eliminate the antenna damage during mixed-phasing operation in L-mode on JET? Does the model predict similar antenna interactions in H-mode? Is there a regime in which the antenna interactions can be avoided in H-mode and yet the monopole antennas are still able to perturb the edge? Can good antenna-plasma coupling be maintained in this regime?

Regarding the first question, there are some possible strategies suggested by the model for reducing antenna interactions in L-mode. One can increase the electric field threshold for arcing (and hence the rf power threshold) by cleaning the antenna surfaces. Another approach would be to try to eliminate the radial current path around the limiters, i.e. to achieve $L_x/\Delta x_L \ll 1$ for the *dipole* antennas which have the weaker sheath voltages. One could reduce $L_x/\Delta x_L \propto (e\Phi/T_e)^{2/3}$ [see Eq. (8)] by limiting the antenna power (and hence the sheath voltage Φ) or by extending the antenna protection limiters (larger Δx_L). However, this strategy is complicated by the fact that we simultaneously require $L_x/\Delta x_L > 1$ for the stronger convective cells at the *monopole* antennas to be able to perturb the edge. Perhaps the best strategy is that one could try to ensure that the ion saturation current is below the minimum current to sustain arcing ($I_s < 1$ A) by reducing the density in the vicinity of the antenna. This could be accomplished by increasing the antenna-plasma separation and/or by increasing the radial extent of the antenna limiters. This last point is also relevant to the second question. In H-mode, the density (and ion saturation current) at the antenna is much lower, and it is therefore easier to avoid triggering arcs. Taking the upper bound on I_{\min} in Eq. (9), the estimates in Sec. 3.4 suggest that a reduction in density of 5–10 near the antenna during the L-H transition might be sufficient to avoid arcs if the monopole power was applied only during the H-mode phase. The mixed-phasing H-mode shot described in Sec. 2 did not show evidence of antenna interactions, consistent with this estimate, but more experimental work needs to be carried out in H-mode before definite conclusions can be drawn.

The need to reduce the density at the antenna to avoid arcing is not inconsistent with the goal of using the rf convection to perturb the plasma edge. The reason is that the parallel scale length $L_{\parallel L}$ between the limiters is typically much shorter than the scale length $L_{\parallel G}$ in the global SOL, so that the large-scale convection can be more important in the global SOL than in the private SOL of the antenna. To make this idea more precise, we define the parallel confinement time $\tau_{\parallel} = L_{\parallel}/c_s$ and the convective eddy time $\tau_c = L_x/v_{Ex}$, where c_s is the sound

speed, v_{Ex} is the radial ExB velocity, and L_x is a typical radial scale length. The regime of interest for these experiments is given by $\tau_{||L} \ll \tau_c < \tau_{||G}$. When this inequality is satisfied, the convection does not flatten the density profile between the antenna protection limiters (allowing reduced density at the antenna), but it can affect the density profile in the global SOL. Whether this regime can be achieved in practice is a quantitative question that is best answered by experiment.

Finally, we note that it is possible to simultaneously reduce sheath interactions at the antenna and to maintain good antenna coupling because the wavelength λ of the fast wave is typically large compared to the radial extent Δx_L of the antenna protection limiter. Sheath effects depend on the density n_a at the antenna (between the antenna protection limiters), whereas the antenna loading is determined by the average density $n = n_{av}$ over a radial scale of approximately $\lambda \approx \delta_i \equiv c/\omega_{pi}$ in front of the antenna. Achieving both reduced sheath interactions and good antenna coupling requires that the local density n_a is smaller than both n_{av} and the fast wave cut-off density [e.g. see the Appendix in Ref. 1]. This is possible when the inequality $\tau_{||L} \ll \tau_c < \tau_{||G}$ is satisfied.

In conclusion, the sheath-driven arcing mechanism described in this paper is consistent with the mixed-phasing experimental results on JET. It suggests that mixed-phasing experiments may be possible in H-mode operation, which is the most interesting application of the idea. Future experiments to investigate the role of monopole rf-driven convection on spreading the divertor heat load, reducing the particle confinement time, and modifying the ELM properties would be of great interest, and may lead to new techniques for optimizing H-mode performance [1, 2].

Acknowledgements

This work was supported by the U.S. Dept. of Energy under DOE Grant No. DE-FG03-97ER54392 and by the EFDA-JET workprogramme. We thank R. Behrisch, V. Bobkov, K. Erents, A. Kaye, R. Lobel, and P. Maget for providing useful information.

References

- ¹ D'Ippolito, D. A., Myra, J. R., Jacquinot, J., and Bures, M., *Phys. Fluids B* **5** (1993) 3603.
- ² D'Ippolito, D. A., and Myra, J. R., *Phys. Plasmas* **7** (2000) 3301.
- ³ Mioduszewski, P., in *Data Compendium for Plasma-Surface Interactions*, R. A. Langley, et al., (IAEA, Vienna, 1984), Nucl. Fusion Special Issue 1984, p. 105.
- ⁴ Behrisch, R., in *Physics of Plasma-Wall Interactions in Controlled Fusion*, D. E. Post and R. Behrisch, Editors, (Plenum Press, New York and London, 1984), p. 495.
- ⁵ Van Nieuwenhove, R., and Van Oost, G., *Plasma Phys. and Controlled Fusion* **34** (1992) 525.
- ⁶ Chodura, R., and Neuhauser, J., in *Proceedings of the Sixteenth EPS Conference on Controlled Fusion and Plasma Heating*, Venice, Vol. **13B**(III) (EPS, 1989) 1089.
- ⁷ D'Ippolito, D. A., Myra, J. R., Bures, M., and Jacquinot, J., *Plasma Phys. and Controlled Fusion* **33** (1991) 607.
- ⁸ Bures, M., Jacquinot, J. et al., *Plasma Phys. and Controlled Fusion* **33** (1991) 937.
- ⁹ Bures, M., Jacquinot, J. et al., *Nucl. Fusion* **32** (1992) 1139.
- ¹⁰ D'Ippolito, D. A., Myra, J. R., Rogers, J. H., et al., *Nucl. Fusion* **38** (1998) 1543.
- ¹¹ Myra, J. R., D'Ippolito, D. A., and Ho, Y. L., *Fusion Eng. Design* **31** (1996) 291.
- ¹² Colas, L., Heuroux, S., Pécoulet, S., Brémond, S., and Bécoulet, M., in *Proceedings of the Fourteenth Topical Conference on Radio Frequency Power in Plasmas*, Oxnard, CA, AIP Conf. Proc. **595** (2001) 134.
- ¹³ Bécoulet, M., Colas, L., Pécoulet, S., Gunn, J., Ghendrih, Ph., Bécoulet, A., and Heuroux, S., *Phys. Plasmas* **9** (2002) 2619.
- ¹⁴ Van Nieuwenhove, R., and Van Oost, G., *J. Nucl. Mater.* **162-164** (1989) 288.
- ¹⁵ Noterdaeme, J.-M., in *Proceedings of the Ninth Topical Conference on Radio Frequency Power in Plasmas*, Charleston, SC, AIP Conf. Proc. **244** (1992) 71.
- ¹⁶ Brambilla, M., and Noterdaeme, J.-M., in *Proceedings of the Seventeenth EPS Conference on Controlled Fusion and Plasma Heating*, Amsterdam, Vol. **14B**(III) (EPS, 1990) 1056.
- ¹⁷ Brambilla, M., Chodura, R., Hoffmann, J., Neuhauser, J., Noterdaeme J.-M., et al., in *Proceedings of the Thirteenth IAEA Conference on Plasma Physics and Controlled Nuclear Fusion Research 1990*, Washington D.C., Vol. **1**, (IAEA, Vienna, 1991) 723.
- ¹⁸ Kaye, A. S., Brown, T., Bhatnagar, V. P., et al., *Fusion Eng. Design* **24** (1994) 1.
- ¹⁹ Perkins, F. W. , *Nucl. Fusion* **29** (1989) 583.
- ²⁰ Myra, J. R., D'Ippolito, D. A., and Gerver, M. J., *Nucl. Fusion* **30**, (1990) 845.
- ²¹ Ryan, P. M., Carter, M. D., Goulding, R. H., Batchelor, D. B., et al., in *Proceedings of the Eleventh Topical Conference on Radio Frequency Power in Plasmas*, Palm Springs, CA, AIP Conf. Proc. **355** (1996) 355.
- ²² Ho, Y.L., Grossmann, W., Drobot, A., Carter, M. D. , Ryan, P. M., and Batchelor, D. B., in *Proceedings of the Tenth Topical Conference on Radio Frequency Power in Plasmas*, Boston, MA, AIP Conf. Proc. **289** (1994) 359.
- ²³ Myra, J. R., D'Ippolito, D. A., and Ho, Y. L., *Fusion Eng. Design* **31** (1996) 291.
- ²⁴ Start, D. F. H., Bell, G., Bhatnagar, V. P., Bures, M., et al., in *Proceedings of the Eleventh Topical Conference on Radio Frequency Power in Plasmas*, Palm Springs, CA, AIP Conf. Proc. **355** (1996) 7.
- ²⁵ D'Ippolito, D. A., and Myra, J. R., *Phys. Plasmas* **3** (1996) 420.
- ²⁶ Lieberman, M. A., *IEEE Trans. Plasma Sci.* **PS-16** (1988) 638.
- ²⁷ Nedospasov, A. V., and Uzdenskiy, D. A., *Contrib. Plasma Phys.* **34** (1994) 478.
- ²⁸ Gunther, K., and Carlson, A., *Contrib. Plasma Phys.* **34** (1994) 484.

Figure Captions

Fig. 1 Time history of D_{α} , radiated power, rf power, line-averaged density and stored energy for the mixed-phasing shot #52673.

Fig. 2 Time history of D_{α} , rf power, edge density, edge T_e and impurity spectral line intensities for the mixed-phasing shot #52673.

Fig. 3 Plot of poloidal sheath voltage distribution, $V(y)$, with 0000 and $0\pi 0\pi$ phasings for three radial positions: one field line just in front (solid curve) and two just in back (dashed curves) of the FS tangency surface. Here, y is measured in meters from the symmetry plane ($y = 0$) and the units of V are arbitrary.

Fig. 4 Normalized throughput current I_t vs. current asymmetry parameter g for fixed normalized rf voltage, $\xi = 10$.

Fig. 5 Sketch of the dc plasma potential vs distance between the anode (left end) and cathode (right end) for the two capacitor plate sheath model. The cases $eV = 0$ and $eV \gg 3T_e$ are shown, where V is the applied potential difference between the plates. The arrows indicate the direction of current flow I_i and I_e , which is taken to be positive. Note that a net current flows to the cathode in the large- V case.

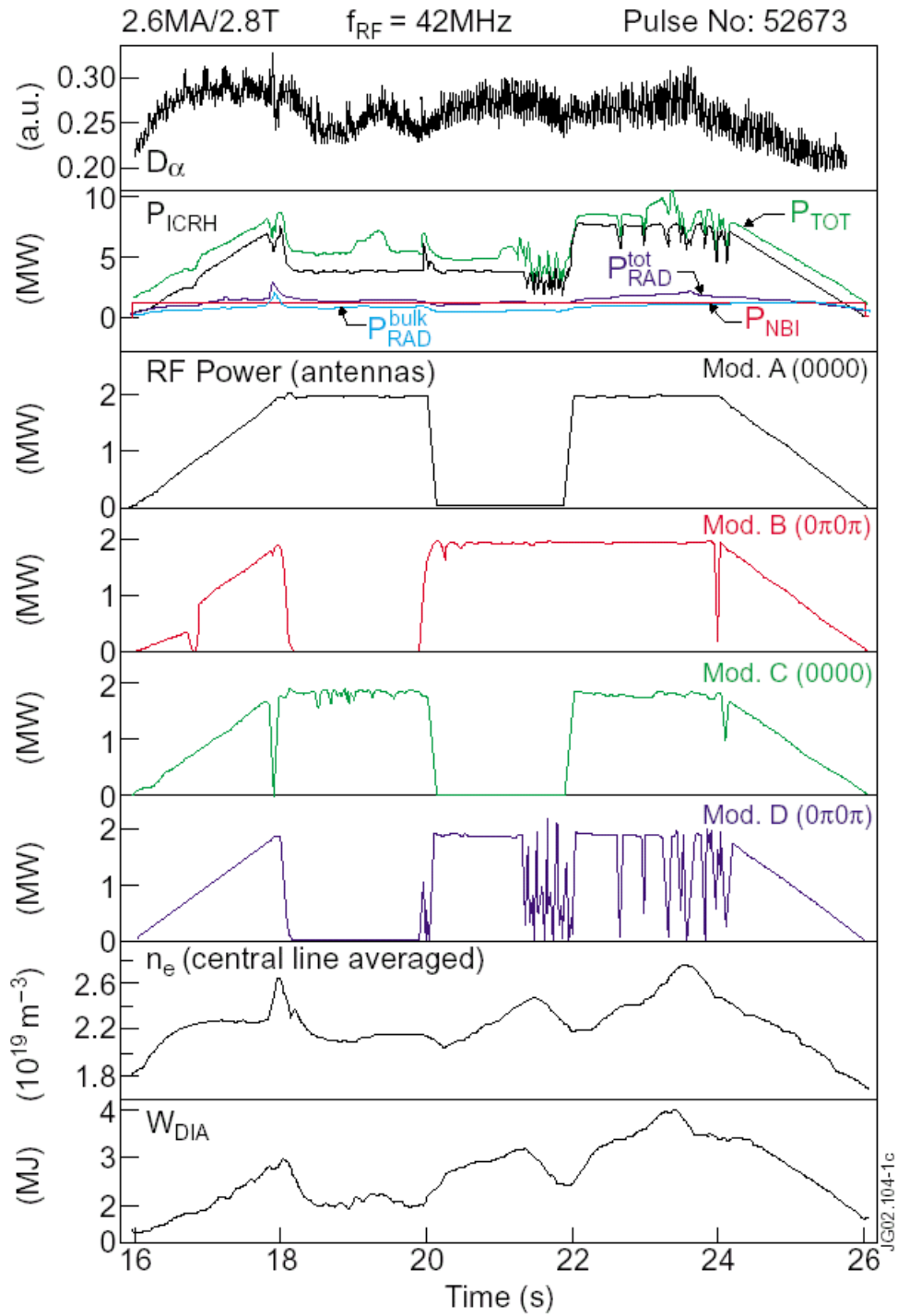


Fig. 1 Time history of D_α , radiated power, rf power, line-averaged density and stored energy for the mixed-phasing shot #52673.

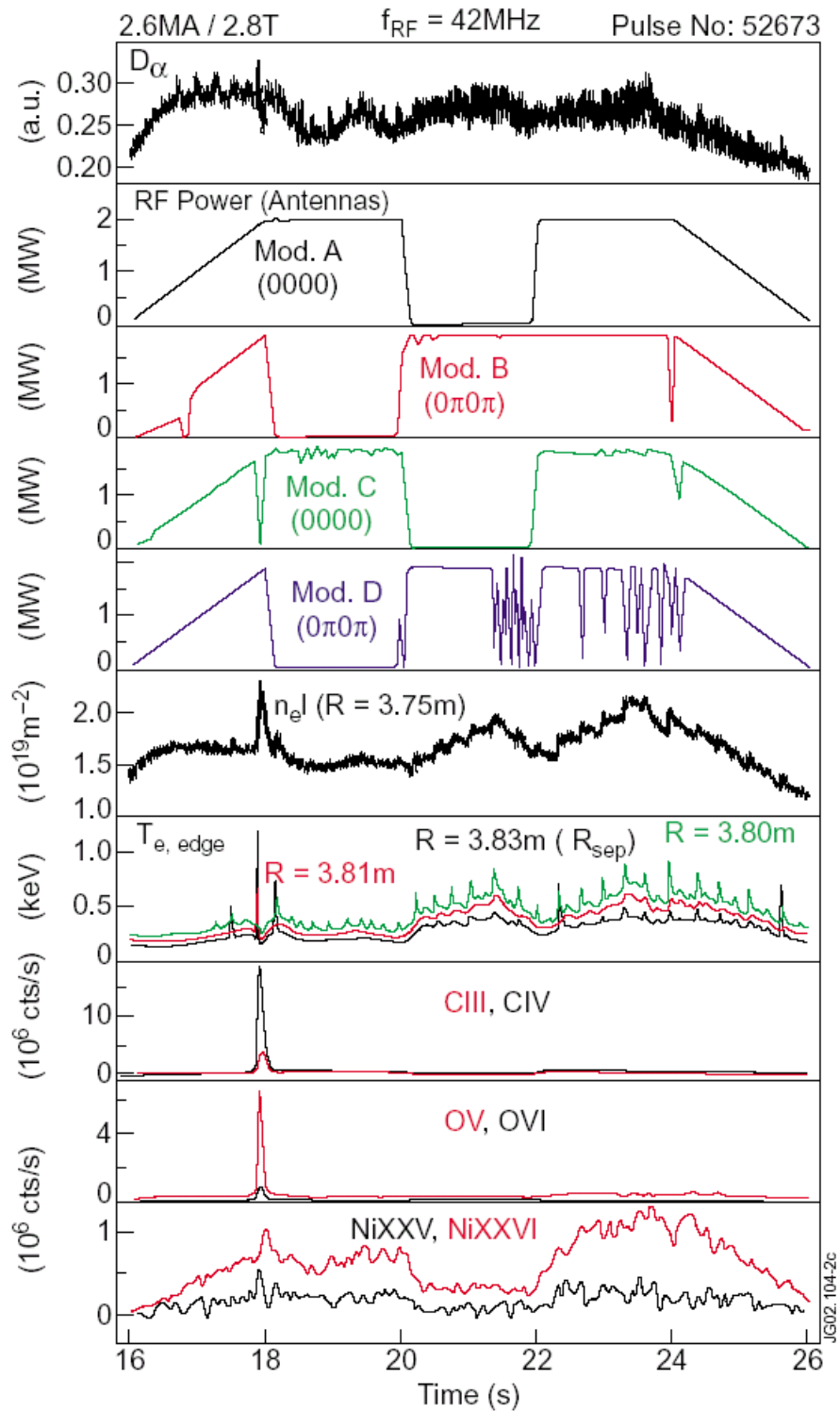


Fig. 2 Time history of D_α , rf power, edge density, edge T_e and impurity spectral line intensities for the mixed-phasing shot #52673.

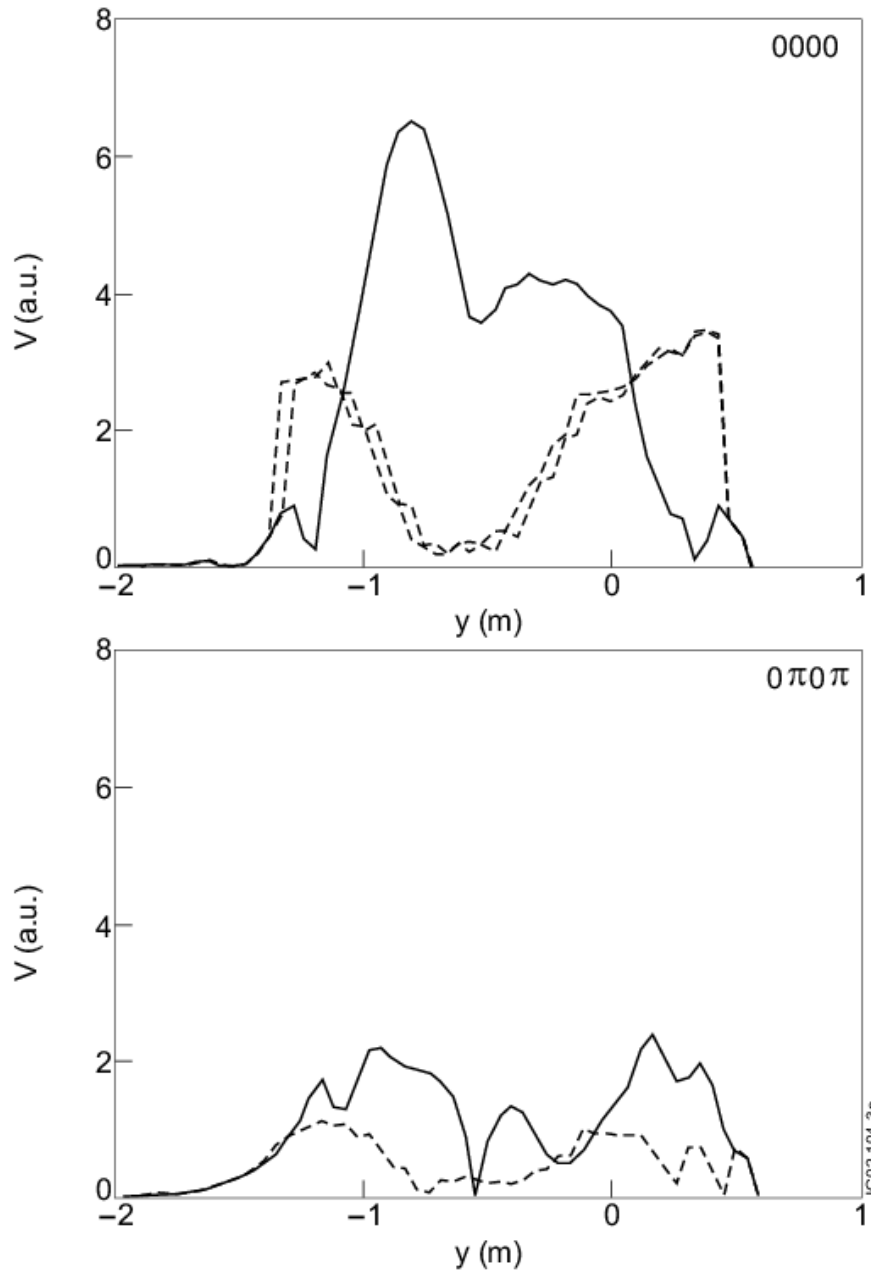


Fig. 3 Plot of poloidal sheath voltage distribution, $V(y)$, with 0000 and $0\pi0\pi$ phasings for three radial positions: one field line just in front (solid curve) and two just in back (dashed curves) of the FS tangency surface. Here, y is measured in meters from the symmetry plane ($y = 0$) and the units of V are arbitrary.

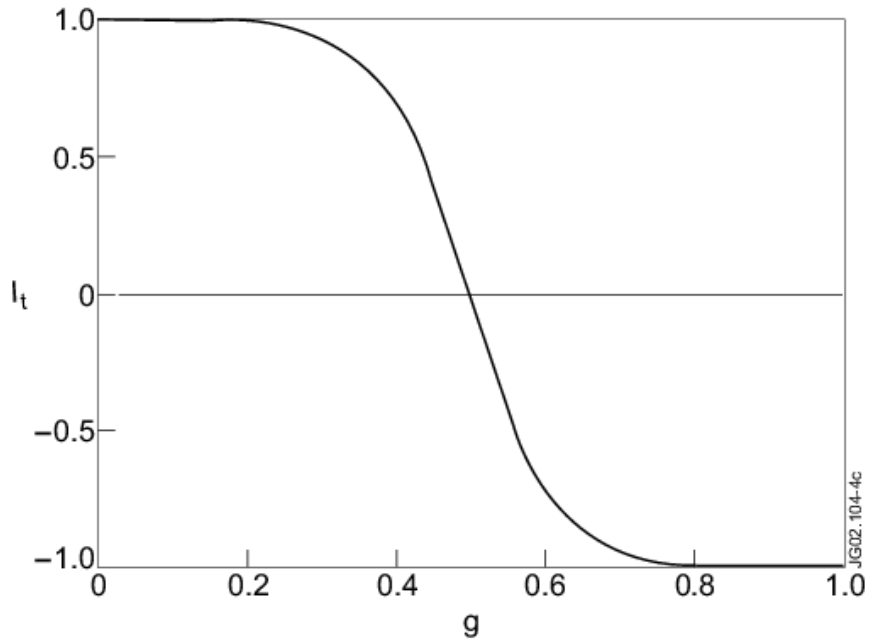


Fig. 4 Normalized throughput current I_t vs. current asymmetry parameter g for fixed normalized rf voltage, $\xi = 10$.

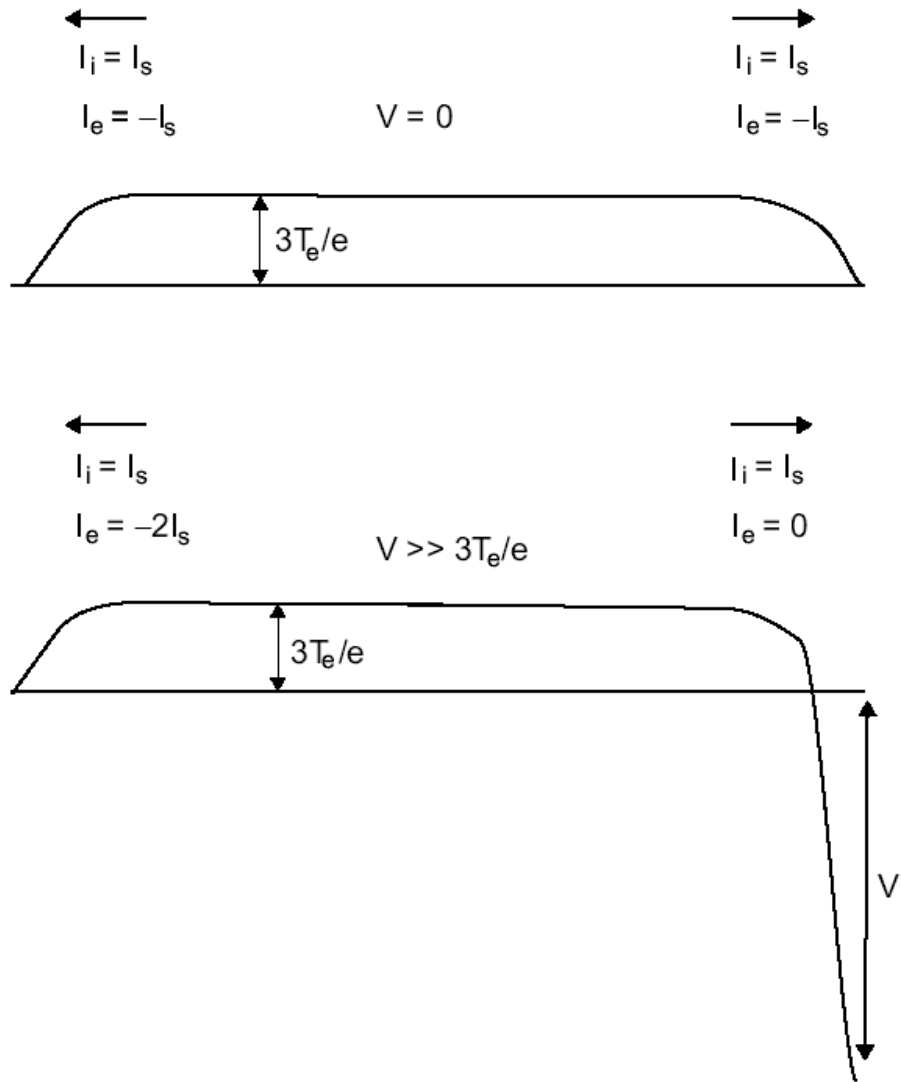


Fig. 5 Sketch of the dc plasma potential vs distance between the anode (left end) and cathode (right end) for the two capacitor plate sheath model. The cases $eV = 0$ and $eV \gg 3T_e$ are shown, where V is the applied potential difference between the plates. The arrows indicate the direction of current flow I_i and I_e , which is taken to be positive. Note that a net current flows to the cathode in the large- V case.